Figure S1. iRIP-seq detects the binding preference on RNAs of PKM2. (A and B) RT-qPCR and western blotting results for PKM2 overexpression in HeLa cells. (C) Western blotting results revealed successful IP of PKM2 in HeLa cells. (D) The hierarchically clustered Pearson correlation matrix was obtained by comparing the transcript expression values for the input and PKM2 IP samples. (E) The scatter plot of read abundance across the reference genome in paired samples showed an enriched preference for PKM2 IP samples. (F) The enriched reads were distributed across the reference genome. *P<0.05, **P<0.01 and ***P<0.001 vs. control or input. iRIP-seq, improved RNA immunoprecipitation sequencing; PMK2, pyruvate kinase M2; RT-qPCR, reverse transcription-quantitative PCR; IP, immunoprecipitation.

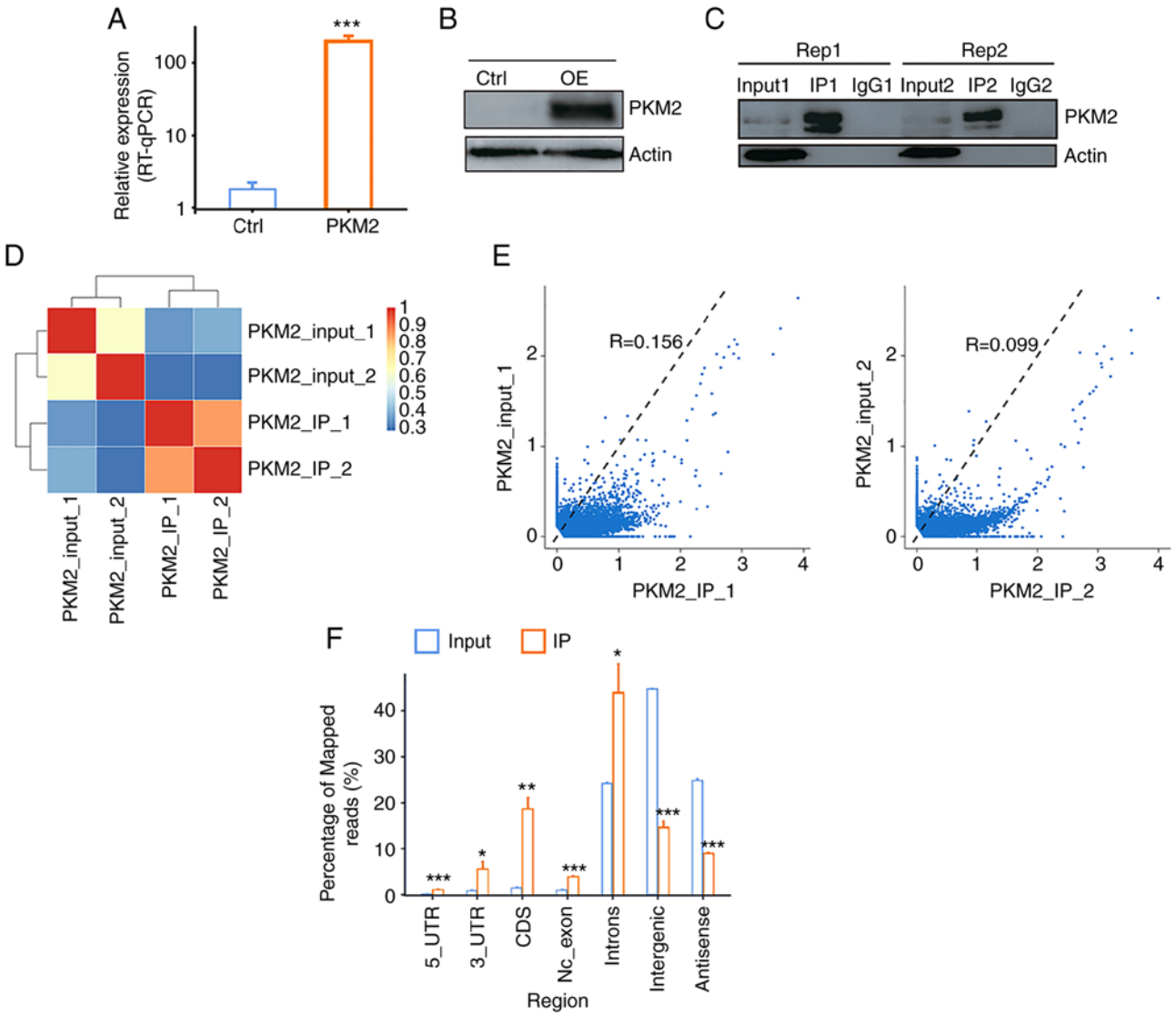

Figure S2. Peak analysis reveals the RNA binding features of PKM2. (A) The peak distribution across the reference genome. (B) The Venn diagram revealed the overlapped peaks in two replicate iRIP-seq samples. (C) The HOMER software was used for motif analysis of the top ten preferred bound motifs of PKM2. (D) The top ten enriched GO biological processes and KEGG pathways of the PKM2-bound genes. PMK2, pyruvate kinase M2; iRIP-seq, improved RNA immunoprecipitation sequencing; GO, Gene Ontology; KEGG, Kyoto Encyclopedia of Genes and Genomes.

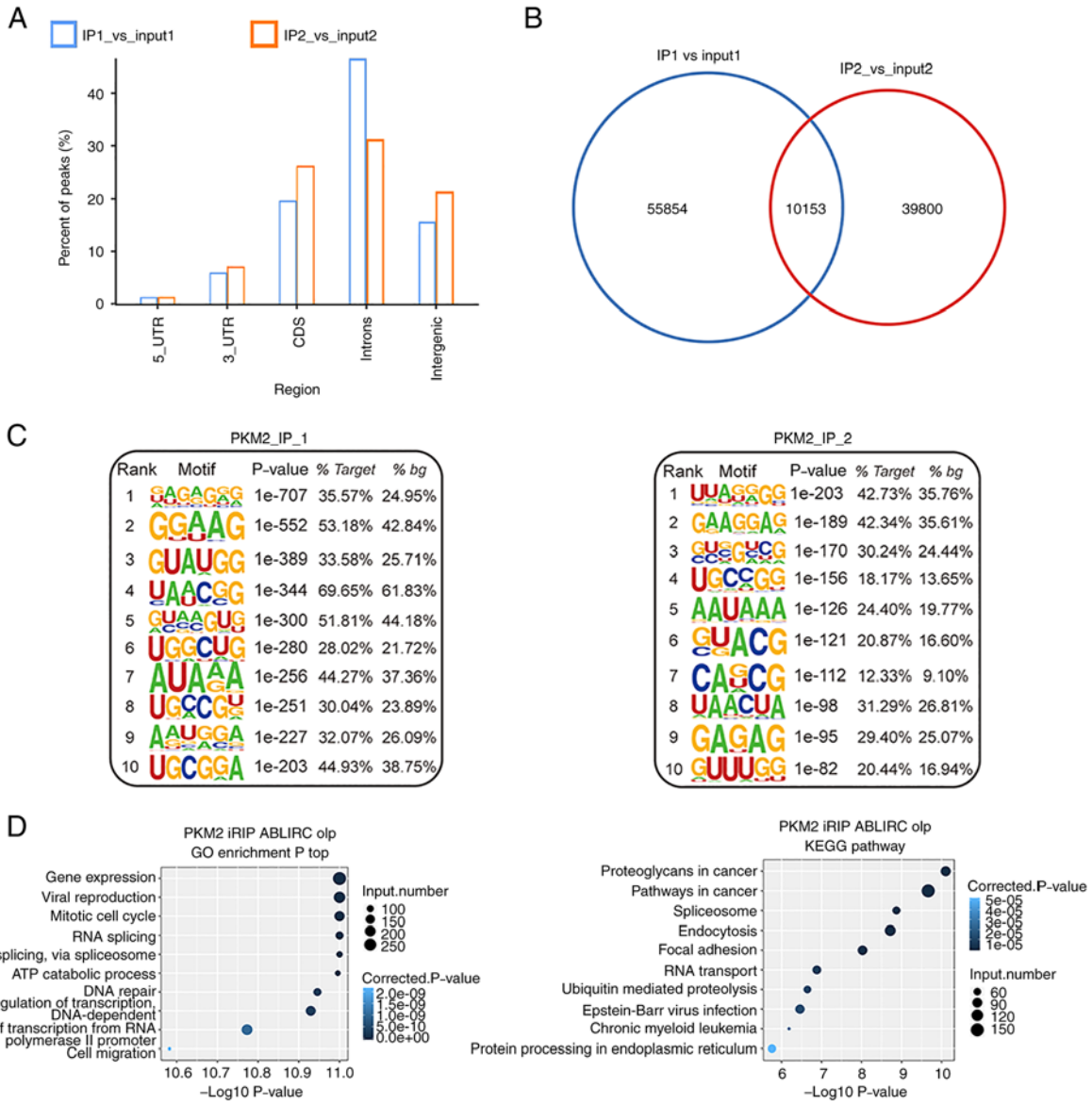

Figure S3. Construction and detection of carrier. (A) RT-qPCR detected the interference efficiency of the sh-lncCCAT1 in HOS and U2OS. (B) RT-qPCR detected the interference efficiency of sh-PKM2. (C) RT-qPCR detected the expression efficiency of pcDNA3.1-lncCCAT1. (D) RT-qPCR and western blotting detected pcDNA3.1-SREBP2 expression in HOS cells. (E) RT-qPCR and western blotting detected the expression of pcDNA3.1-SREBP2-WT and pcDNA3.1-SREBP2^{T610A} in HOS cells. **P<0.01 vs. sh-NC or pcDNA3.1. RT-qPCR, reverse transcription-quantitative PCR; sh-, short hairpin; PMK2, pyruvate kinase M2; lncCCAT1, lncRNA colon cancer associated transcript-1; SREBP2, sterol regulatory element-binding protein 2; WT, wild-type; NC, negative control.

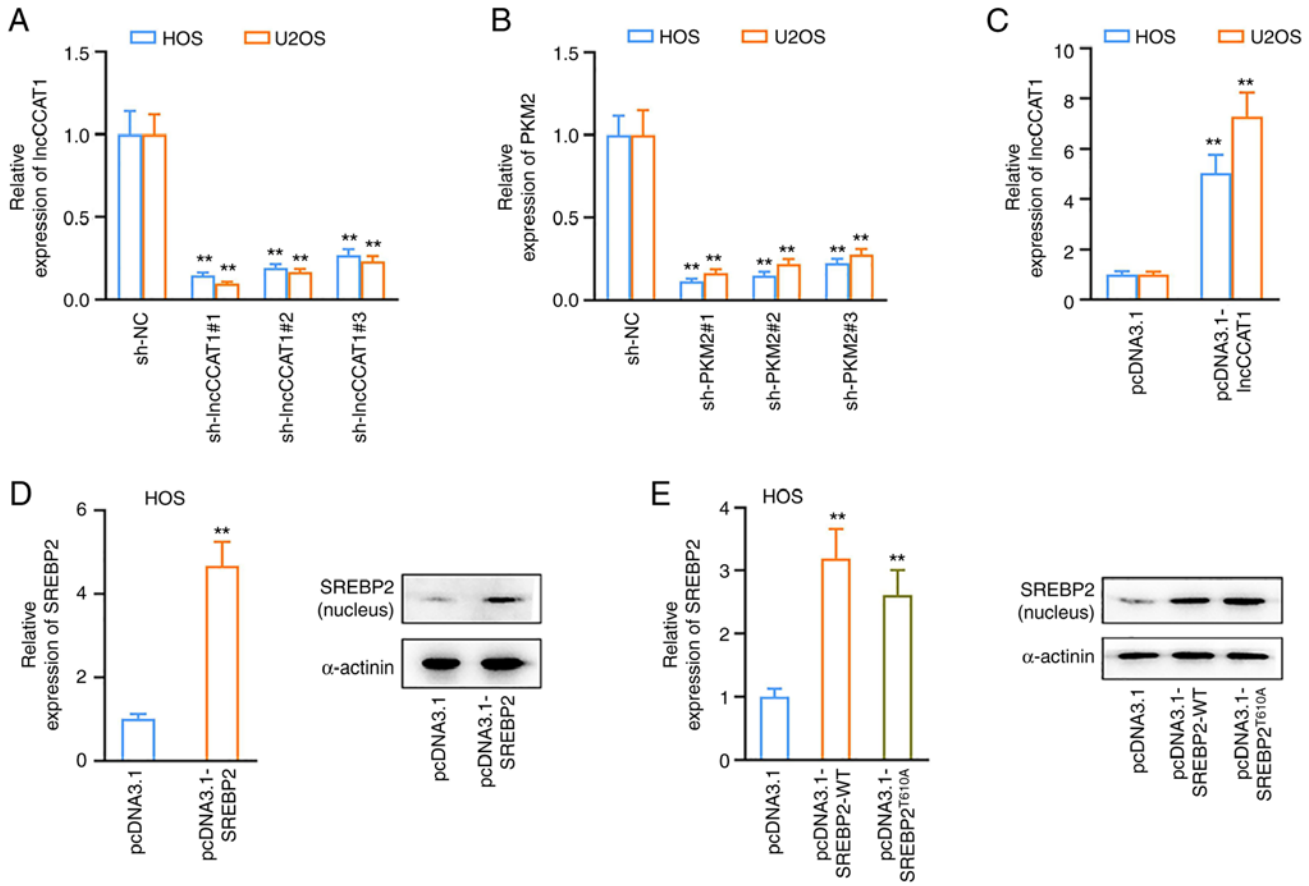

Figure S4. Construction and detection of carrier. (A) After detecting interference with lncCCAT1 using Seahorse XF Extracellular Flux Analyzers, the ECAR of HOS and U2OS cells was decreased, (B) the OCR was increased, and (C) the level of NAPDH/NAPD$^+$ was decreased. **P<0.01 vs. sh-NC. lncCCAT1, lncRNA colon cancer associated transcript-1; ECAR, extracellular acidification rate; OCR, oxygen consumption rate; sh-, short hairpin; NC, negative control.

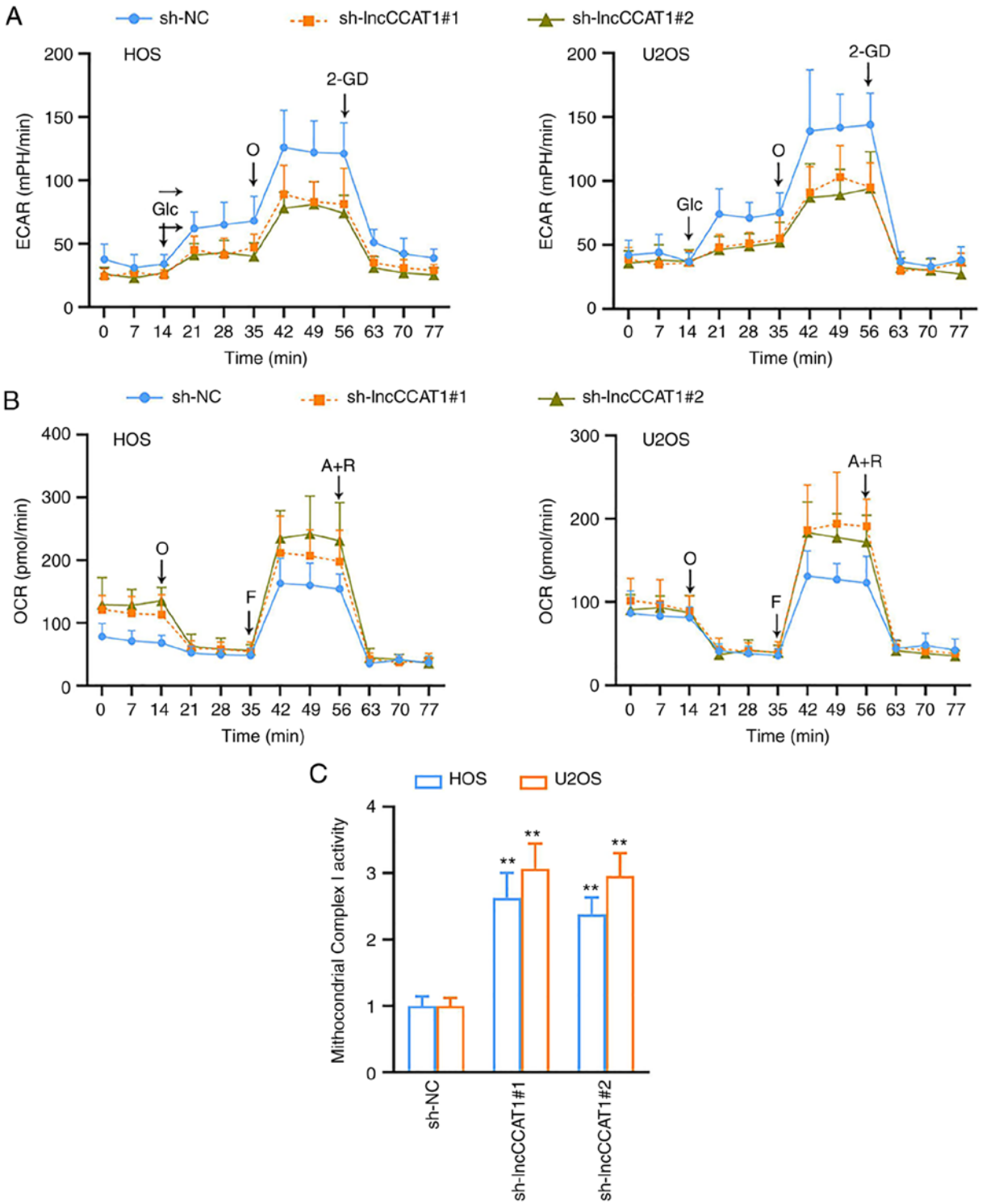

Figure S5. LncCCAT1 promotes the proliferation of OS cells through PKM2. (A) RIP assay verified the binding effect of lncCCAT1 and PKM2. (B) RNA pulldown assay verified that lncCCAT1 could pulldown PKM2. (C) Overexpression of lncCCAT1 promoted the proliferation of OS cells, and after the interference with PKM2, reduced proliferation of OS cells as detected by CCK-8, (D) reduced number of positive cells of EdU assay, (E) and decreased cell clones of clonal formation assay were detected. **P<0.01. lncCCAT1, lncRNA colon cancer associated transcript-1; OS, osteosarcoma; PMK2, pyruvate kinase M2; RIP, RNA immunoprecipitation; CCK-8, Cell Counting Kit-8; EdU, 5-ethynyl-20-deoxyuridine; sh-, short hairpin; NC, negative control.

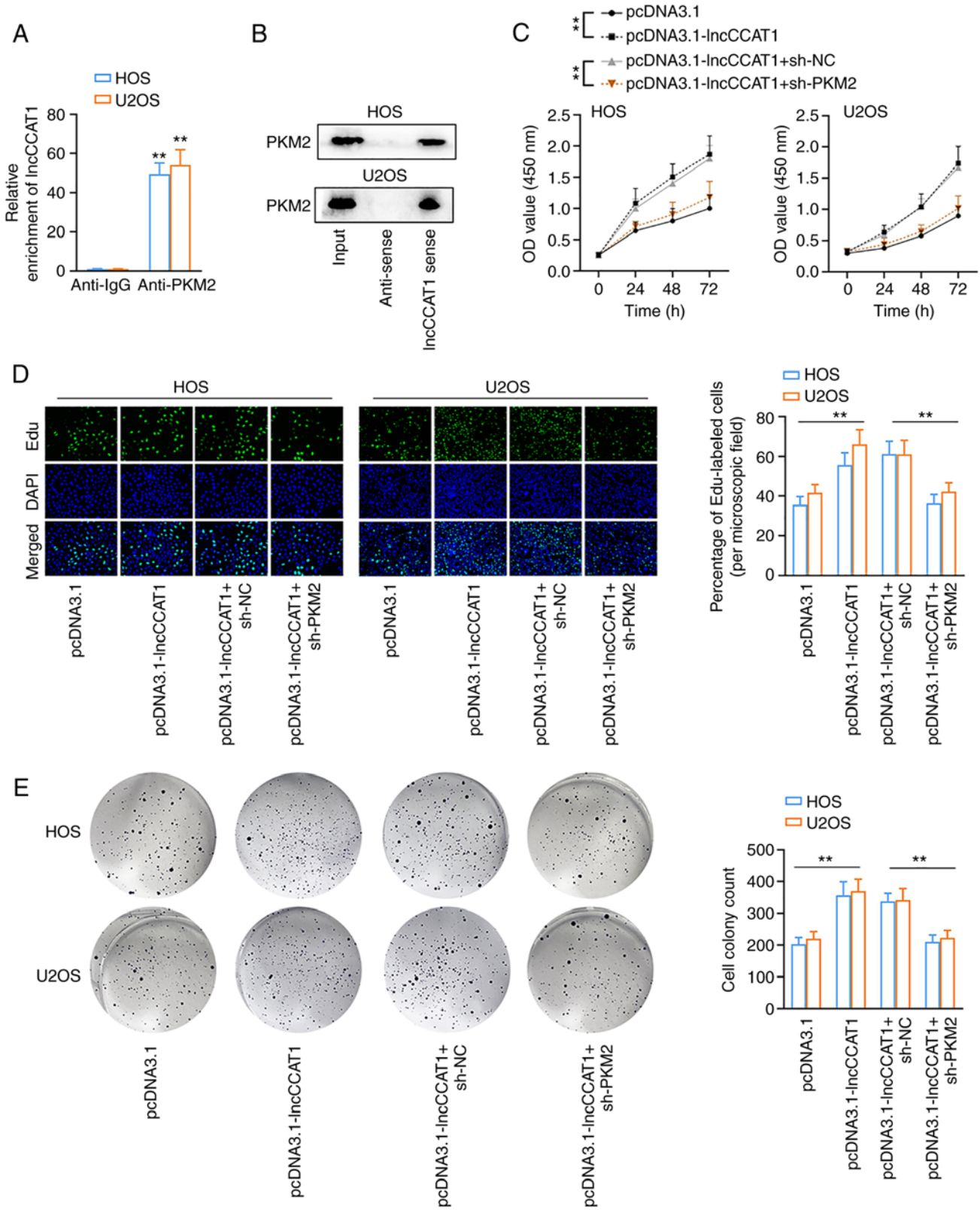

Figure S6. LncCCAT1 promotes the Warburg effect of OS cells through PKM2. (A and B) Following overexpression of lnCCCAT1, the glucose content in cells increased; then, after interference with PKM2, glucose and lactic acid decreased. (C-E) Following overexpression of lncCCAT1, the Seahorse XF Extracellular Flux Analyzer detected that the ECAR was increased, the OCR was decreased, and the ECAR/OCR was increased. On this basis, PKM2 was disrupted, and it was determined that ECAR was decreased, the OCR was increased, and the ECAR/OCR was decreased. (F-K) Following overexpression of lncCCAT1, intracellular levels of NAPDH/NAPD^{+} and GSH increased, the intracellular levels of ATP, and the mitochondrial complex I activity decreased, the intracellular levels of glucose 6-phosphate and 3-PG increased. After the aforementioned treatment, PKM2 was disrupted again, and the results revealed that the intracellular levels of NAPDH/NAPD^{+} and GSH decreased, the intracellular levels of ATP and the mitochondrial complex I activity increased, and the intracellular levels of glucose 6-phosphate and 3-PG decreased. **P<0.01. lncCCAT1, lncRNA colon cancer associated transcript-1; OS, osteosarcoma; PMK2, pyruvate kinase M2; ECAR, extracellular acidification rate; OCR, oxygen consumption rate; GSH, glutathione; sh-, short hairpin; NC, negative control.

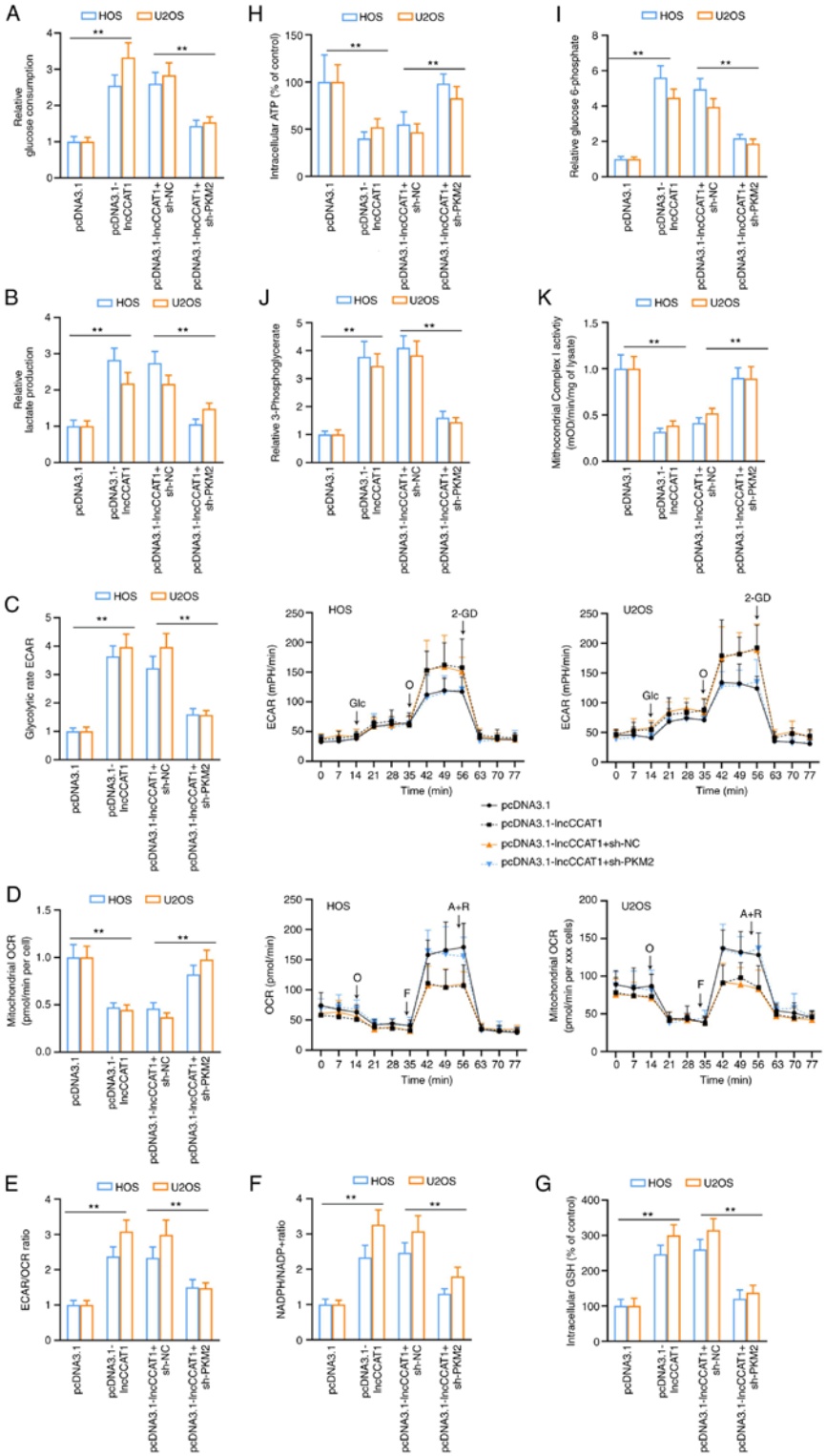

Figure S7. LncCCAT1 promotes the proliferation of OS cells through PKM2. Following PKM2 interference, HOS and U2OS cells were treated with α-amanitin, and the expression levels of lncCCAT1 and GAPDH in the nucleus were detected by RT-qPCR. The results revealed that PKM2 could stabilize lncCCAT1. **P<0.01. lncCCAT1, lncRNA colon cancer associated transcript-1; OS, osteosarcoma; PMK2, pyruvate kinase M2; RT-qPCR, reverse transcription-quantitative PCR; sh-, short hairpin; NC, negative control.

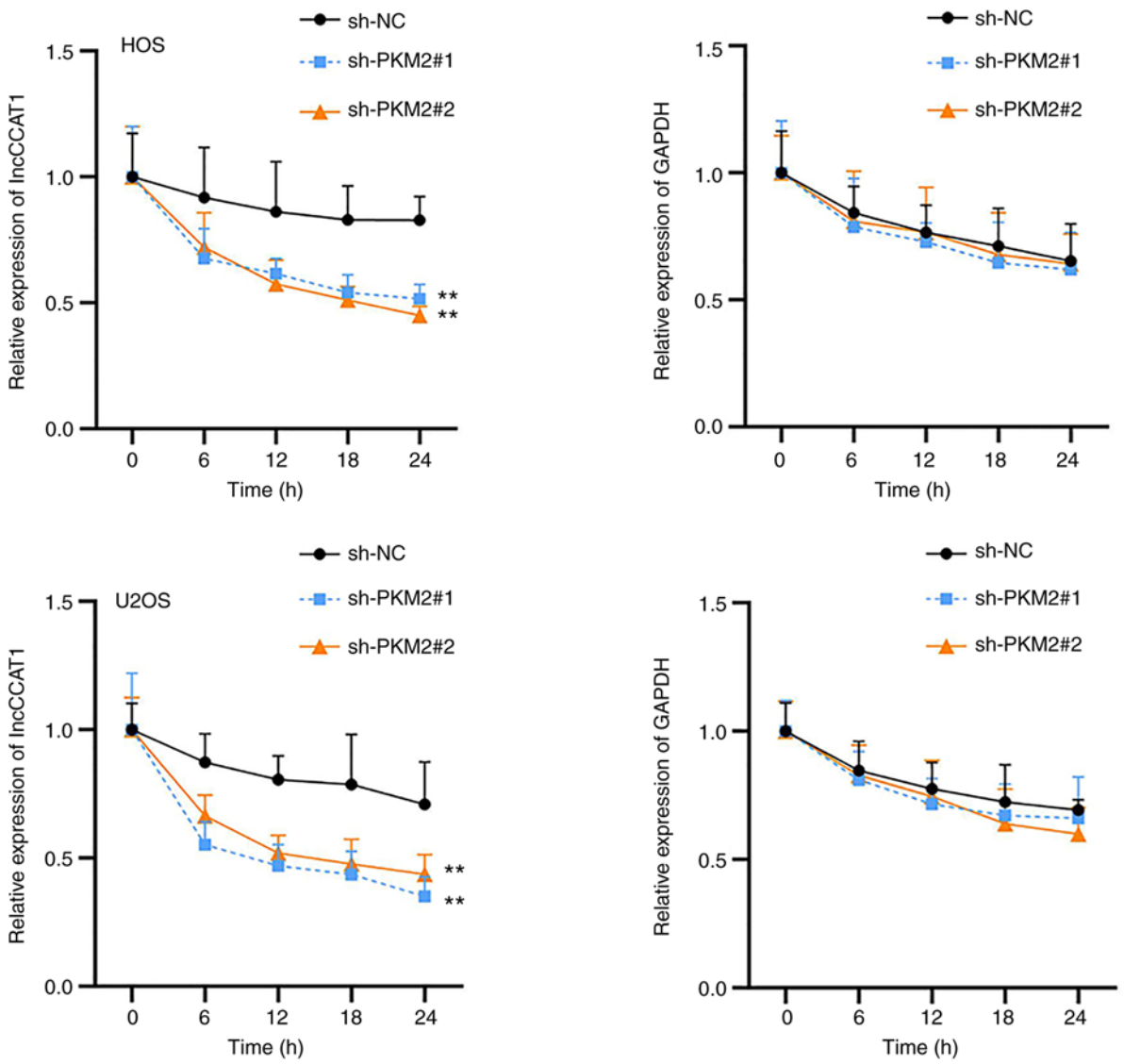

Figure S8. Prediction of phosphorylation sites of SREBP2. (A) Co-IP assay showed that interfering lncCCAT1 did not affect the interaction between PKM2 and SREBP2. (B) Websites were used to predict the phosphorylation sites of SREBP2, and the two most likely phosphorylation sites in the range of 600-630 were T610 and S627. SREBP2, sterol regulatory element-binding protein 2; lncCCAT1, lncRNA colon cancer associated transcript-1; PMK2, pyruvate kinase M2.